ARCHIVES OF ELECTRICAL ENGINEERING VOL. 62(1), pp. 123-140 (2013)

DOI 10.2478/aee-2013-0009

Phenomenon of the eddy current exceeding the exciting magnetomotive force

ROMAN VOGEL

TU Dortmund University, Chair of Electrical Drives and Mechatronics
Emil-Figge-Str. 70, 44227 Dortmund, Germany
e-mail: roman.vogel@tu-dortmund.de

(Received: 18.06.2012, revised: 14.11.2012)

Abstract: Harmonic flux penetrating solid conductive material causes eddy currents inside. It seems plausible that its magnitude does not exceed the exciting magnetomotive force (mmf). However, under certain circumstances the opposite occurs. This article deals with a special case in which the eddy current is approximately 13% higher than the exciting mmf. An analytical field solution, a finite element calculation and a measurement proving this phenomenon are presented. A special flux linkage is turned out to be the reason for this phenomenon. Finally, another example with higher pronounced mmf-exceeding in a coil is presented.

Key words: analytic field solution, eddy current, magnetic coupling, phenomenon

1. Introduction

Magnetic field coupling between electrical circuits is fundamental for electromagnetic devices with inductive energy transfer (transformers, electrical machines, sheet forming, inductive heating, etc.). For the design of such devices complicated calculation methods like the Finite-Element-Method (FEM) are required due to the complex geometry and saturation effects. However, the results produced by such models are complicated and it is at least necessary to check if they are physically plausible.

We concentrate on the plausibility of eddy currents, which occur in many devices and are therefore an important and intensively studied issue [1-5]. The main focus of eddy-current-studies is usually the power loss produced. In this article the eddy current magnitude is analysed. In time-harmonic case the magnitude of eddy current is expected to be lower than the exciting mmf. Such intuitive assumption is based on the classical equivalent circuit of a transformer and it is in accordance with daily experience. This article, however, shows that the opposite can be true.

An example of eddy current which measurably exceeds the primary current (approx. 13%) is analysed. At first a parametrical analytical solution for the particular example is derived. Then the influence of the parameters on the eddy current magnitude is investigated. For one case with a markedly high exceeding, the analytical result is verified by FEM. Additionally an experimental setup is presented which definitely proves the phenomenon of eddy current exceeding the exciting magnetomotive force.

2. Analytical model

An extensive review of analytical approaches for the calculation of two-dimensional electromagnetic fields is presented in [6]. One of the analytical solutions (transformer reactance, derived by Rogowski) can be modified for calculating the eddy currents in the arrangement depicted in Figure 1.

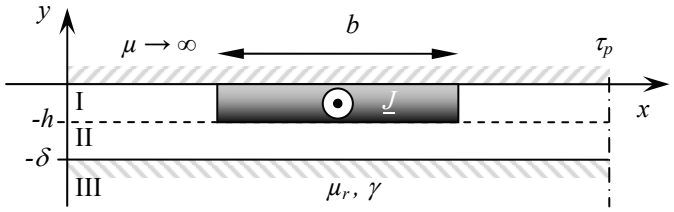

Fig. 1. Arrangement for analytical calculation of eddy current

The model represents one of the anti-cyclical repetitive magnetic poles with the pitch τ_p. The space above the x-axis is highly permeable and non-conducting (orthogonal magnetic field immediately under it). Below the axis, in the adjacent air gap with the width δ a stranded conductor with the height h and width b is arranged which is fed by harmonic current density

$$\underline{J} = \frac{\hat{J}}{\sqrt{2}} \cdot e^{j\omega t}. \tag{1}$$

Under the air gap a solid material with constant relative permeability μ_r and constant conductivity γ follows. We define the band regions I, II, and III which is beneficial for the mathematical formulation of governing field equations.

2.1. Field equations and method of resolution

The aforementioned field problem can be solved by using the magnetic vector potential A which expresses the magnetic flux density $\vec{B}$ in the following way [7]:

$$\vec{B} = \nabla \times \vec{A} = \nabla \times \left(A \cdot \vec{e}_z\right) \quad \Rightarrow \quad B_x = \partial A / \partial y, \;\; B_y = -\partial A / \partial x. \tag{2}$$

Thus $\vec{B}$ satisfies Maxwell's Equation $\nabla \cdot \vec{B} = 0$ because of $\nabla \cdot \nabla \times = 0$ [8]. Now the field is defined by a scalar function $A(x, y, t)$ instead of a vector $\vec{B}$ (x, y, t). Due to harmonic ex-

citation and linearity of materials the vector potential is harmonic and will therefore be represented by phasor $\underline{A}(x, y)$ according to:

$$A(x,y,t) = \mathrm{Re}\left\{ \sqrt{2}\,\underline{A}(x,y)\cdot e^{j\omega t} \right\}. \tag{3}$$

Distribution of the complex vector potential $\underline{A}$ is governed by general field equation [7]

$$\Delta\underline{A}(x,y) = -\mu\cdot\underline{J}(x,y). \tag{4}$$

The exciting current density $\underline{J}$ is defined by the winding inside of region I and disappears inside of region II. In the space of region III the current is driven by the induced electrical field $E = -\partial A/\partial t$ [7], which yields according to $J = \gamma \cdot E$:

$$J_{\mathrm{III}} = -\gamma\cdot\partial A_{\mathrm{III}}/\partial t \quad\Rightarrow\quad \underline{J}_{\mathrm{III}} = -j\omega\gamma\underline{A}_{\mathrm{III}}. \tag{5}$$

Thus, the following field equations result for the three band regions I, II, and III:

$$\begin{aligned} \Delta\underline{A}_{\mathrm{I}} &= -\mu_0 J(x), && \text{region I (winding inside airgap)} \\ \Delta\underline{A}_{\mathrm{II}} &= 0, && \text{region II (airgap)} \\ \Delta\underline{A}_{\mathrm{III}} &= j\omega\mu_r\mu_0\gamma\underline{A}_{\mathrm{III}}, && \text{region III (solid material).} \end{aligned} \tag{6}$$

Current density $J(x)$ inside region I is a step function which we expand in a Fourier series

$$J(x) = \sum_n J_n \sin(nkx), \quad n = 1,3,5,... \tag{7}$$

with coefficients

$$J_n = \frac{\hat{J}}{\sqrt{2}}\frac{4}{n\pi}\sin\left(n\frac{\pi}{2}\right)\sin\left(\frac{nkb}{2}\right) \tag{8}$$

and wave number of the fundamental wave

$$k = \frac{\pi}{\tau_p}. \tag{9}$$

Due to linearity of material the superposition principle is allowed. This means that every single summand $J_n\sin(nkx)$ excites a field content $\underline{A}_n(x, y)$ which may be determined separately. In order to gain the solution for $\underline{A}_n$, separation of the variables $\underline{A}_n = \underline{Y}_n(y)\cdot X_n(x)$ is applied. The factor $\underline{X}_n(x)$ equals $\sin(nkx)$ which results from the excitation summand $J_n\sin(nkx)$. This yields following solution statements for the regions I, II, and III:

$$\begin{aligned} \underline{A}_{\mathrm{I}} &= \sum_n \underline{Y}_{\mathrm{I}n}(y)\cdot\sin(nkx) \\ \underline{A}_{\mathrm{II}} &= \sum_n \underline{Y}_{\mathrm{II}n}(y)\cdot\sin(nkx) \qquad n = 1,3,5,... \\ \underline{A}_{\mathrm{III}} &= \sum_n \underline{Y}_{\mathrm{III}n}(y)\cdot\sin(nkx) \end{aligned} \tag{10}$$

Now, the functions $\underline{Y}_{\mathrm{I}\,n}$, $\underline{Y}_{\mathrm{II}\,n}$, and $\underline{Y}_{\mathrm{III}\,n}$ have to be determined. By inserting $\underline{A}_{\mathrm{I}}$ from (10) and $J(x)$ from (7) into the field equation (6) of region I we obtain

$$\sum_n \left(-(nk)^2 \underline{Y}_{\mathrm{I}n} + \frac{\partial^2 \underline{Y}_{\mathrm{I}n}}{\partial y^2} \right) \cdot \sin(nkx) = -\mu_0 \sum_n J_n \sin(nkx). \tag{11}$$

Comparing the coefficients of $\sin(nkx)$ yields the governing equation for $\underline{Y}_{\mathrm{I}\,n}$

$$\frac{\partial^2 \underline{Y}_{I\,n}}{\partial y^2} - (nk)^2 \underline{Y}_{I\,n} = -\mu_0 J_n\,, \tag{12}$$

the solution of which is

$$\underline{Y}_{I\,n} = \underline{C}_{I\,n} \cdot e^{nky} + \underline{C}'_{I\,n} \cdot e^{-nky} + \frac{\mu_0 J_n}{(nk)^2}. \tag{13}$$

The unknown coefficients $\underline{C}$ will be determined later using boundary conditions. Analogously we obtain the governing equations for $\underline{Y}_{\mathrm{II}\,n}$ and $\underline{Y}_{\mathrm{III}\,n}$ by inserting (10) into (6):

$$\frac{\partial^2 \underline{Y}_{II\,n}}{\partial y^2} - (nk)^2 \underline{Y}_{II\,n} = 0, \quad \frac{\partial^2 \underline{Y}_{III\,n}}{\partial y^2} - \underline{\beta}_n^2 \underline{Y}_{III\,n} = 0, \tag{14}$$

where:

$$\underline{\beta}_n = \sqrt{(nk)^2 + j\omega\mu_r\mu_0\gamma}. \tag{15}$$

Following solution statements result for $\underline{Y}_{\mathrm{I}\,n}$, $\underline{Y}_{\mathrm{II}\,n}$, and $\underline{Y}_{\mathrm{III}\,n}$:

$$\begin{aligned} \underline{Y}_{\mathrm{I}n} &= \underline{C}_{\mathrm{I}n} \cdot e^{nky} + \underline{C}'_{\mathrm{I}n} \cdot e^{-nky} + \frac{\mu_0 J_n}{(nk)^2}, \\ \underline{Y}_{\mathrm{II}n} &= \underline{C}_{\mathrm{II}n} \cdot e^{nky} + \underline{C}'_{\mathrm{II}n} \cdot e^{-nky}, \\ \underline{Y}_{\mathrm{III}n} &= \underline{C}_{\mathrm{III}n} \cdot e^{\underline{\beta}_n y} + \underline{C}'_{\mathrm{III}n} \cdot e^{-\underline{\beta}_n y}. \end{aligned} \tag{16}$$

2.2. Analytical field solution

The six unknown coefficients $\underline{C}$ in (16) result from the boundary conditions. Since the magnetic field is orthogonal immediately below the x-axis and does not diverge at infinity we obtain:

$$\begin{aligned} \underline{B}_{x\mathrm{I}}\big|_{y=0} &= \left.\frac{\partial \underline{A}_{\mathrm{I}}}{\partial y}\right|_{y=0} = 0 \Rightarrow \underline{C}_{\mathrm{I}n} = \underline{C}'_{\mathrm{I}n}\,, \\ \lim_{y\to-\infty} &\left|\underline{Y}_{\mathrm{III}}(y)\right| \neq \infty \Rightarrow \underline{C}'_{\mathrm{III}n} = 0\,. \end{aligned} \tag{17}$$

Normal component of B and tangential component of H are continuous at the boundaries I/II and II/III which yields:

$$\begin{aligned} \underline{B}_{y\mathrm{I}} &= \underline{B}_{y\mathrm{II}}\big|_{y=-h} \\ \underline{H}_{x\mathrm{I}} &= \underline{H}_{x\mathrm{II}}\big|_{y=-h} \\ \underline{B}_{y\mathrm{II}} &= \underline{B}_{y\mathrm{III}}\big|_{y=-\delta} \\ \underline{H}_{x\mathrm{II}} &= \underline{H}_{x\mathrm{III}}\big|_{y=-\delta} \end{aligned} \quad \Rightarrow \quad \begin{aligned} \underline{Y}_{\mathrm{I}n} &= \underline{Y}_{\mathrm{II}n}\big|_{y=-h} \\ \frac{\partial \underline{Y}_{\mathrm{I}n}}{\partial y} &= \frac{\partial \underline{Y}_{\mathrm{II}n}}{\partial y}\bigg|_{y=-h} \\ \underline{Y}_{\mathrm{II}n} &= \underline{Y}_{\mathrm{III}n}\big|_{y=-\delta} \\ \frac{\partial \underline{Y}_{\mathrm{II}n}}{\partial y} &= \frac{1}{\mu_r}\frac{\partial \underline{Y}_{\mathrm{III}n}}{\partial y}\bigg|_{y=-\delta} \end{aligned} \tag{18}$$

We evaluate these conditions according to (16) considering (17) and obtain an equation system for determination of the remaining four coefficients:

$$\begin{pmatrix} \dfrac{\mu_0 J_n}{(nk)^2} \\ 0 \\ 0 \\ 0 \end{pmatrix} = \begin{bmatrix} -2\cosh(nkh) & e^{-nkh} & e^{nkh} & 0 \\ 2\sinh(nkh) & e^{-nkh} & -e^{nkh} & 0 \\ 0 & e^{-nk\delta} & e^{nk\delta} & -e^{-\underline{\beta}_n \delta} \\ 0 & e^{-nk\delta} & -e^{nk\delta} & -\dfrac{\underline{\beta}_n}{nk\mu_r} e^{-\underline{\beta}_n \delta} \end{bmatrix} \cdot \begin{pmatrix} \underline{C}_{\mathrm{I}n} \\ \underline{C}_{\mathrm{II}n} \\ \underline{C}'_{\mathrm{II}n} \\ \underline{C}_{\mathrm{III}n} \end{pmatrix} \tag{19}$$

Coefficient $\underline{C}_{\mathrm{III}n}$ required for calculation of the field in region III is determined by Cramer's rule [8] which yields:

$$\underline{C}_{\mathrm{III}n} = \frac{\dfrac{\mu_r \mu_0 J_n e^{\underline{\beta}_n \delta}}{nk \sinh(nk(\delta - h))}}{\coth(nkh)(\underline{\beta}_n \coth(nk(\delta - h)) + nk\mu_r) + (\underline{\beta}_n + nk\mu_r \coth(nk(\delta - h))}. \tag{20}$$

Now to obtain the field solution in solid region III we evaluate $\underline{C}_{\mathrm{III}n}$=0 (see (17)) in $\underline{Y}_{\mathrm{III}n}$ (see (16)) and put it in $\underline{A}_{\mathrm{III}}$ (see (10)), which results in:

$$\underline{A}_{\mathrm{III}}(x, y) = \sum_n \underline{C}_{\mathrm{III}n} \cdot e^{\underline{\beta}_n y} \sin(nkx), \quad n = 1,3,5,..., \tag{21}$$

where $\underline{C}_{\mathrm{III}n}$, $\underline{\beta}_n$, and k are coefficients according to (20), (15), and (9).

2.3. Eddy current

In order to calculate the eddy current, we integrate the current density, which results from (21) according to (5), in one pole pitch of the solid material:

$$\underline{I}_2 = \int_{-\infty}^{-\delta} \int_{0}^{\tau_p} \underline{J}_{\mathrm{III}} \cdot dx \cdot dy =$$

$$-j\omega\gamma \int_{-\infty}^{-\delta} \sum_n \left(\underline{C}_{\mathrm{III}n} \cdot e^{\underline{\beta}_n y} \underbrace{\int_0^{\pi/k} \sin(nkx) \cdot dx}_{2/n\pi} \right) \cdot dy = -j \frac{2\omega\gamma}{k} \sum_n \left[\frac{\underline{C}_{\mathrm{III}n}}{n\underline{\beta}_n} \cdot e^{\underline{\beta}_n y} \right]_{y=-\infty}^{y=-\delta} \tag{22}$$

This leads to the following expression of the eddy current:

$$\underline{I}_2 = -\frac{j2\omega\gamma}{k} \sum_n \frac{\underline{C}_{\mathrm{III}n}}{n\underline{\beta}_n} \cdot e^{-\underline{\beta}_n \delta}. \tag{23}$$

3. Parameter influence on the current ratio

The current ratio I_2/I_1, which we calculate from (23) and (1):

$$\frac{I_2}{I_1} = \left| -\frac{j2\omega\gamma}{k} \sum_n \frac{\underline{C}_{\mathrm{III}n}}{n\underline{\beta}_n} \cdot e^{-\underline{\beta}_n \delta} \right| / \left(\frac{\hat{J}}{\sqrt{2}} bh \right) \tag{24}$$

is frequency dependent. It converges to zero for low frequency (low voltage induction inside the solid conductor) and to a constant value for high frequencies. In particular the curve in between is dependent on parameters. When the normalized winding width b/τ_p, gap width δ/τ_p and relative permeability μ_r of the solid conductor decrease, a peak arises and the ratio I_2/I_1 exceeds the value of one which seems not to be plausible. Figure 2 depicts exemplarily the curve of a reference arrangement with the parameters according to Table 1 and shows the influences of b/τ_p, δ/τ_p, μ_r and conductivity γ. A change of γ shifts the frequency of the peak, but does not reduce the peak height.

Table 1. Parameters of the Reference Arrangement

Symbol	Quantity	Value
τ_p	pole pitch	20 mm
h	winding height	0.199 mm
b	winding width	0.4 mm
δ	air gap width	0.2 mm
μ_r	relative permeability of the solid conductor	1
γ	electrical conductivity of the solid conductor	$36 \cdot 10^6$ S/m

This phenomenon contradicts the experience with eddy currents and magnetically coupled circuits and will therefore be verified by FEM and measurement.

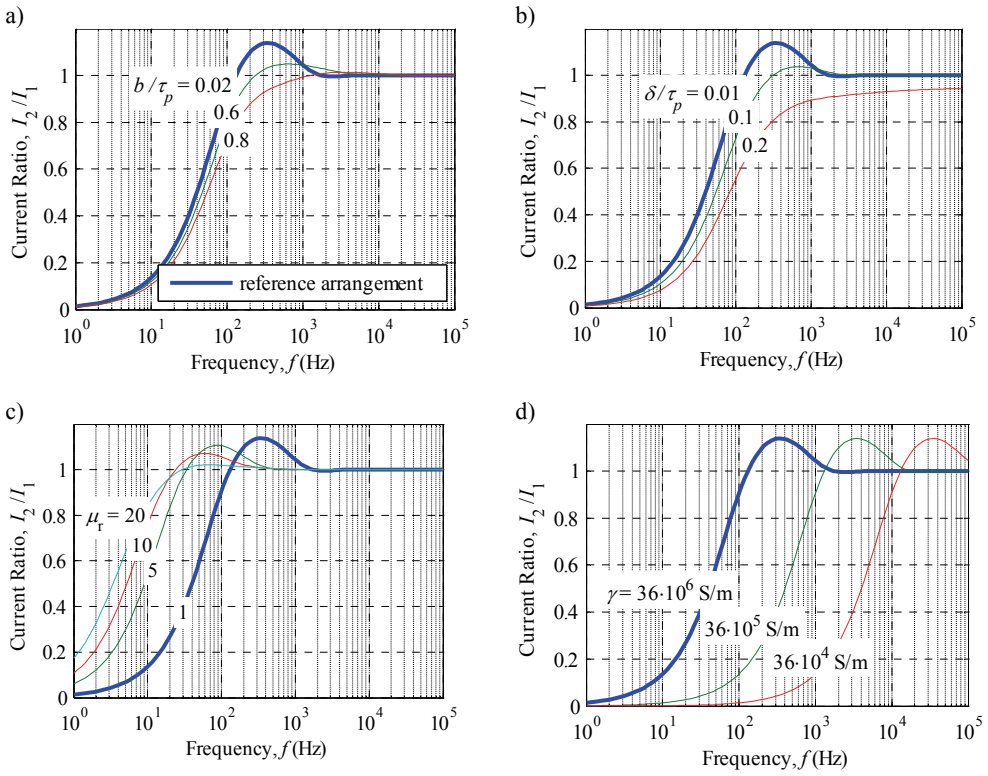

Fig. 2. Current ratio exceeding the value of one. The phenomenon occurs depending on parameters b/τ_p, δ/τ_p, and μ_r, see a), b), c). A change of the conductivity γ shifts the frequency of the peak, see d)

4. Verification of the phenomenon

In this section two FE-models (A, B) and a test setup will be introduced. The geometry of the test setup differs from that of the analytical model for a certain reason (see Section 4.2). It definitely reveals the phenomenon, however, the measured curve deviates from the analytic one because of the different geometry. Therefore, the verification requires two FE-models. FE-model A verifies the analytic curve, FE-model B verifies the measured one.

4.1. FE-models

In order to create the FE-models we use commercial software FLUX 2D®. FE-model A (see Fig. 3) is built up according to the parameters of the reference arrangement (see Table 1). It includes one half of the pole pitch due to symmetry. Since $b \approx \delta$, the gap between winding and solid conductor is neglected in the model. The boundary conditions are orthogonal magnetic fields on the x-axis as well as on the left vertical line and tangential fields on both other borders. The solid conductor (infinitely high in the analytical model) is cut at the height

of 80 mm, followed by air. Due to small primary-coil-cross-section a very fine mesh results which is sufficient for the frequency range dealt with.

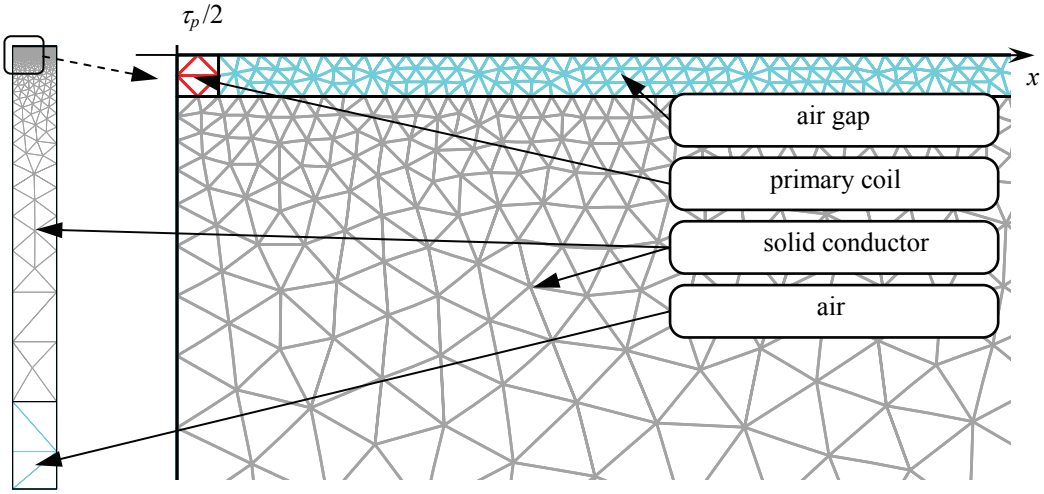

Fig. 3. FE-model A

FE-model B, with the function to verify the measured curve, is depicted in Figure 4. It includes a quarter section of the test setup due to symmetry. The only difference is the rectangular cross section of the primary coil in the FE-model B which is circular in the test setup. The influence on the current ratio resulting from this difference is, however, negligible because of the small size of the primary-coil-cross-section. The boundary conditions are an orthogonal magnetic field on the upper horizontal line and tangential magnetic fields on the other three borders. Like in the FE-model A a very fine mesh results from geometry.

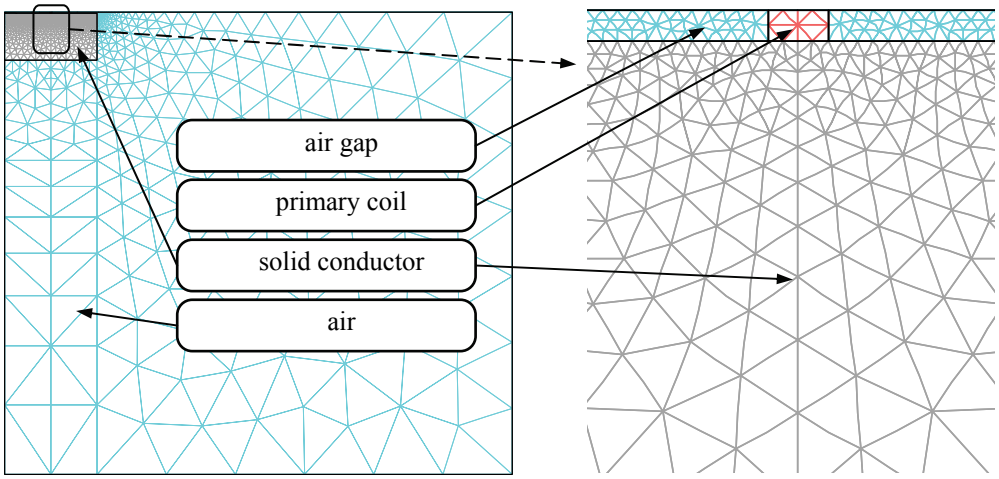

Fig. 4. FE-model B

We will use the current ratio I_2/I_1 calculated from FE-models A and B to verify the analytic and measured curve in Section 4.3.

4.2. Measurement

The test assembly (see Fig. 5) is constructed according to the reference arrangement (see Table 1). An aluminium bar with a 2 mm gap subdividing it into forward and return conductor serves as solid conductor. Therewith only two pole pitches are included. The height is set to 10 mm which approximately equals double skin depth at the expected frequency of the current-ratio-peak ($f \approx 350$ Hz, see Fig. 2 => skin depth ≈ 4.5 mm).

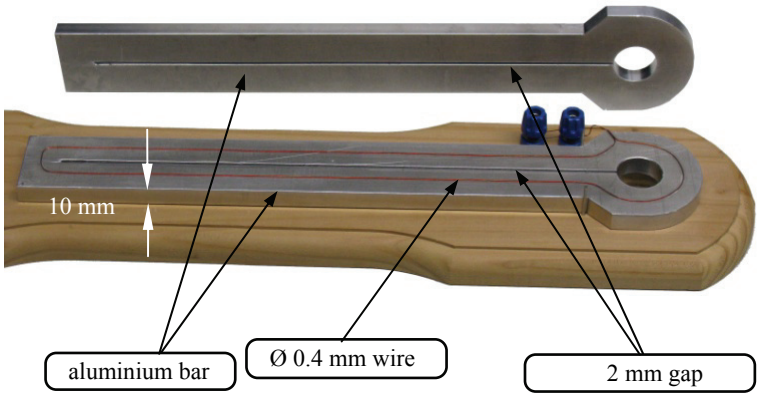

Fig. 5. Test assembly

In order to assure the orthogonal magnetic field at the *x*-axis according to Figure 1, the test assembly is constructed symmetrically (primary coil between two aluminium bars). A circular copper wire (Ø 0.4 mm) is used as primary coil, which is nearly equivalent to the rectangular coil of the reference arrangement. In particular the decisive air gap width is the same.

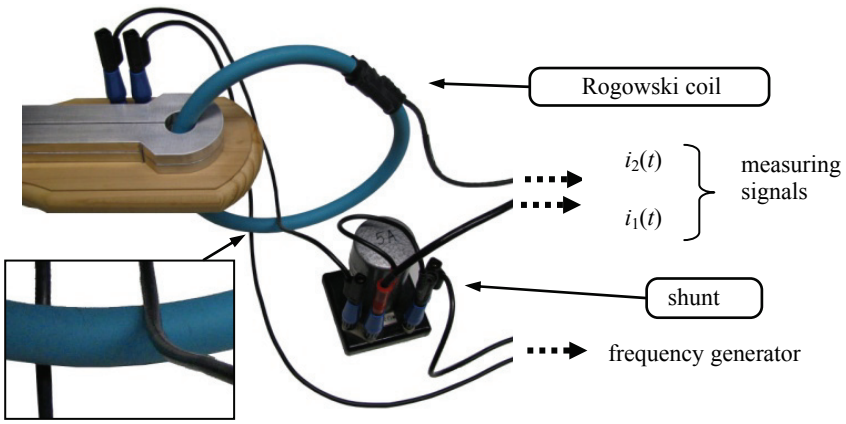

Fig. 6. Test setup

The test setup is depicted in Figure 6. The primary coil is fed by a frequency generator with sinusoidal current $I \approx 1.5$ A and continuously growing frequency ($f = 20$ Hz…500 Hz within 50 s). The primary current is measured using a shunt. At the same time the resulting eddy current is measured by a Rogowski coil. Since a Rogowski coil measures the sum of currents it is closed around, and the primary coil of the test assembly inevitably is part of it, one supply cable is additionally enclosed for compensation (see Fig. 6).

Both currents are recorded using a digital oscilloscope (20 kHz sampling rate => 40 samples/period at 500 Hz). In order to extract the frequency curve I_2/I_1 from both measured signals, we use successive peaks in pairs. From these the data curves of rms values I_2 and I_1, and the corresponding frequency f are calculated by $I = (i_{\max} - i_{\min})/2\sqrt{2}$ and $f = 1/|2(t_{\max} - t_{\min})|$ respectively.

4.3. Comparison of curves

Figure 7 compares the four current ratio curves, resulting from the FE-models A and B, the analytical calculation and the measurement.

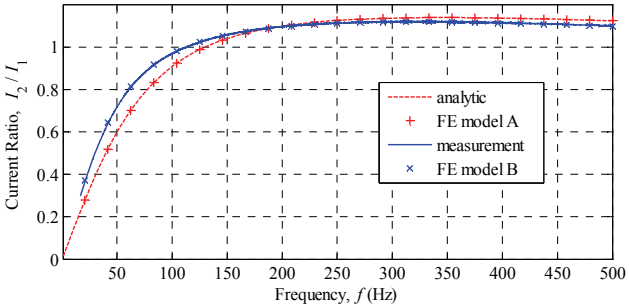

Fig. 7. Current ratio as a function of frequency

The accuracy of the analytic curve is verified by its accordance with the curve of FE-model A. The measured curve deviates from the analytic one. However, it coincides with the curve of the FE-model B, confirming the accuracy of the measurement.

So the analytic method (complex vector potential and resolution by separation of variables) as well as the FEM prove the phenomenon to be true. A physical interpretation is not trivial due to the complexity of the analytical solution and will therefore be dealt with further.

5. Physical interpretation

In order to find a physical interpretation for the phenomenon the ratio of the eddy current and the primary current which serves as exciting mmf is derived regarding the eddy current arrangement as a linear network. This is composed of the primary winding and solid material which can be treated as two circuits with magnetic coupling. In the ac-case the solid material can be treated as a circuit despite its infinite depth. It behaves like a short-circuited solid con-

ductor with finite depth (see agreement between analytic curve and FE model A in Fig. 7) because the current-carrying cross section is finite due to skin effect.

Now we regard the eddy current arrangement from Figure 1. Due to the linearity of material the resulting electromagnetic field, voltages and currents are harmonic and can therefore be expressed by phasors, in particular both currents: $\underline{I}_1$ – primary current (exciting current); $\underline{I}_2$ – secondary current (short-circuit current).

Voltages and currents of both circuits are linearly linked by a frequency dependent matrix (impedance matrix):

$$\begin{pmatrix} \underline{U}_1 \\ \underline{U}_2 \end{pmatrix} = \begin{bmatrix} \underline{Z}_{11}(\omega) & \underline{Z}_{12}(\omega) \\ \underline{Z}_{21}(\omega) & \underline{Z}_{22}(\omega) \end{bmatrix} \cdot \begin{pmatrix} \underline{I}_1 \\ \underline{I}_2 \end{pmatrix}. \tag{25}$$

The secondary circuit is short-circuited ($\underline{U}_2 = 0$ V) so the according Equation in (25) yields the current ratio I_2 / I_1:

$$0 = \underline{Z}_{21} \cdot \underline{I}_1 + \underline{Z}_{22} \cdot \underline{I}_2 \Rightarrow I_2 / I_1 = \left| \underline{Z}_{21} / \underline{Z}_{22} \right|. \tag{26}$$

The case $I_2 / I_1 > 1$ evidently occurs when the magnitude of the mutual impedance $|\underline{Z}_{21}|$ exceeds the magnitude of the self impedance $|\underline{Z}_{22}|$ which seems to be a contradiction. However, this can be the case we will prove and depict in the following section by regarding an arrangement with a one-dimensional magnetic field and, at first, without skin effect. Afterwards we will analyse the influence of the skin effect on the current ratio. In the end we will see another example with the current ratio strongly exceeding the value of one.

5.1. Arrangement with one-dimensional field

We further regard an arrangement consisting of one primary winding (current i_1) and one secondary winding (current i_2) which are surrounded by a nonconductive back iron with high permeability (see Fig. 8). Forward conductors of both windings are on the right of the y-axis, return conductors on the left. The relation between axial length l_z of the arrangement, height h and width b of the secondary winding is: $l_z >> b >> h$.

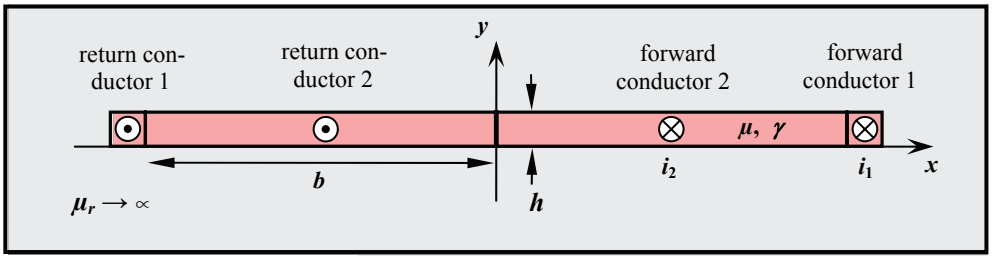

Fig. 8. A winding with narrow cross section (forward and return conductor 2) and big axial length enveloped by another winding (forward and return conductor 1). A back iron with high permeability surrounds both windings

The fields resulting inside forward and return conductor 2 are symmetrical and one-dimensional:

$$\begin{aligned} \vec{H} &= H_y(x,t)\cdot\vec{e}_y \qquad H_y(x,t) = \;\; H_y(-x,t) \\ \vec{E} &= \;\; E_z(x,t)\cdot\vec{e}_z \qquad E_z(x,t) = -E_z(-x,t). \end{aligned} \tag{27}$$

The crucial analogy of this arrangement with that in Figure 1 is the linkage of the flux tubes which is higher for the primary winding than for the secondary one (see Fig. 11).

5.1.1. Secondary conductors without skin effect

If the secondary conductors consist of a large number of mutually insulated, transposed strands, skin effect does not occur inside. Then the complex impedances $\underline{Z}_{21}$ and $\underline{Z}_{22}$ which determine the current ratio according to (26) can be expressed as follows:

$$\begin{aligned} \underline{Z}_{21} &= \qquad j\omega L_{21} \\ \underline{Z}_{22} &= R_2 + j\omega L_{22} \end{aligned} \quad \Rightarrow \quad \frac{I_2}{I_1} = \frac{\left|j\omega L_{21}\right|}{\left|j\omega L_{22} + R_2\right|} \overset{\omega >> \frac{R_2}{L_{22}}}{\rightarrow} \frac{L_{21}}{L_{22}} \; . \tag{28}$$

When frequency increases the current ratio tends to the quotient of the mutual inductance L_{21} and of the self-inductance L_{22}. These can be determined from dc-field of the secondary winding (see Fig. 9).

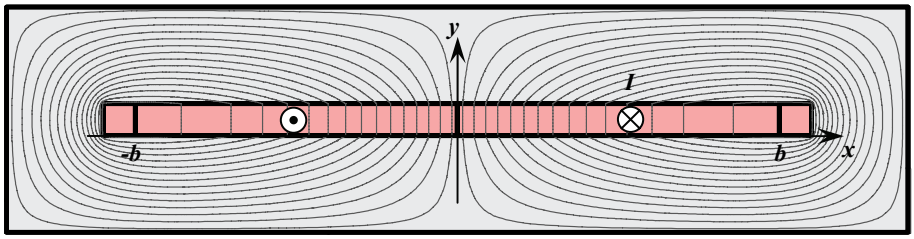

Fig. 9. Flux lines produced by a **constant** secondary current $i_2 = I$. Primary current $i_1 = 0$ A

For further calculations the surface ratio function is defined:

$$a_2(x) = 1 - \frac{x}{b}, \quad 0 \le x \le b. \tag{29}$$

It describes the relative cross-section portion of forward conductor 2, limited by variable position x and the boundary $x = b$. Now we apply Ampere's law on a closed flux line crossing forward conductor 2 and, considering that magnetic field disappears inside the back iron, obtain an expression for the magnetic field inside:

$$H_y(x) = a_2(x)\frac{I}{h}, \qquad 0 \le x \le b, \qquad i_1 = 0\,\text{A}, i_2 = I. \tag{30}$$

Based on (30) we calculate the flux portion of a flux tube

$$d\,\Phi \;\; = B_y\, l_z dx = \mu_0\, H_y(x) l_z dx = \mu_0\, a_2(x)\frac{I}{h} l_z dx \tag{31}$$

and its contribution to the flux linkages Ψ_1 and Ψ_2 of the primary and the secondary winding which depend on the corresponding cross-section-portions a_1 and a_2 enclosed by this flux tube:

$$\begin{array}{lll} d\Psi_1 = & a_1 \cdot d\Phi & a_1 = 1 \\ d\Psi_2 = & a_2(x) \cdot d\Phi & a_2 \le 1 \end{array} \quad \Rightarrow \quad d\Psi_2 \le d\Psi_1 \text{ (!)}. \tag{32}$$

Distribution of the flux linkages $d\Psi_1/dx$, $d\Psi_2/dx$ and resulting values Ψ_1, Ψ_2:

$$\begin{aligned} \Psi_1 &= \int d\Psi_1 = 2 \cdot \int_0^b \mu_0 \frac{I}{h} l_z \left(1 - \frac{x}{b}\right) dx = \mu_0 \frac{I}{h} l_z b, \\ \Psi_2 &= \int d\Psi_2 = 2 \cdot \int_0^b \left(1 - \frac{x}{b}\right) \cdot \mu_0 \frac{I}{h} l_z \left(1 - \frac{x}{b}\right) dx = \frac{2}{3} \mu_0 \frac{I}{h} l_z b. \end{aligned} \tag{33}$$

are depicted in Figure 10.

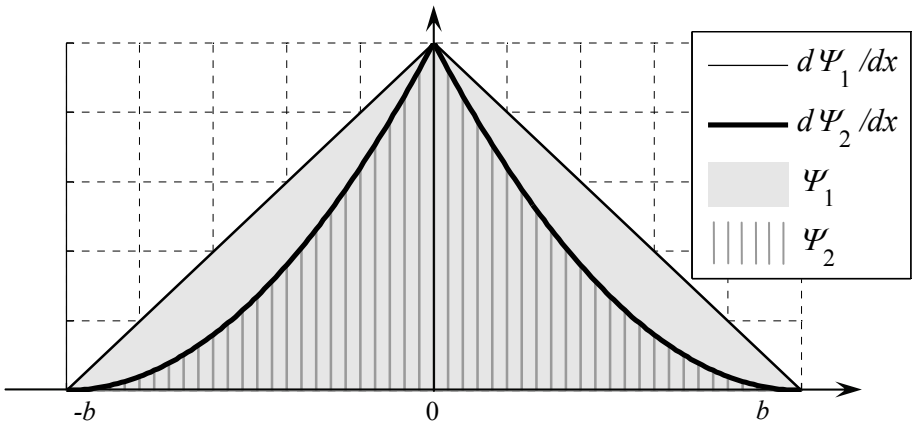

Fig. 10. Flux linkage of the primary and secondary winding

We can see that the linkage of the flux with the field-producing secondary winding is lower than with the open-circuited primary winding. Consequently the self inductance L_{22} is lower (!) than the mutual inductance L_{12} which is equal to L_{21}:

$$\begin{aligned} L_{12} &= \frac{\Psi_1}{I} = \mu \frac{l_z b}{h} \\ L_{22} &= \frac{\Psi_2}{I} = \frac{2}{3} \mu \frac{l_z b}{h} < L_{12} = L_{21}, \end{aligned} \tag{34}$$

and the current ratio (28) becomes greater than one at high frequency:

$$\frac{I_2}{I_1} \overset{\omega >> \frac{R_2}{L_{22}}}{\rightarrow} \frac{L_{21}}{L_{22}} = 1{,}5. \tag{35}$$

For verification the mutual inductance L_{21} can be calculated from the dc-field of the primary winding, resulting analogously to (30) from Ampere's law:

$$H_y(x) = H_y = \frac{I}{h}, \qquad 0 \le x \le b, \qquad i_1 = I,\ i_2 = 0\,\text{A}\,, \tag{36}$$

as follows:

$$L_{21} = \frac{\Psi_2}{I} = \frac{1}{I}\int a_2(x)\cdot d\Phi = \frac{1}{I}\cdot 2\cdot \int_0^b \left(1-\frac{x}{b}\right)\mu\frac{I}{h} l_z\, dx = \mu\frac{l_z b}{h} = L_{12}. \tag{37}$$

So the current or rather the mmf of a short-circuited coil can noticeably exceed the exciting mmf. In the presented arrangement this is due to the fact that the tubes of magnetic flux generated by the secondary winding link the secondary winding only partially ($a_2 < 1$, interior flux) and the primary winding fully ($a_1 = 1$, exterior flux). Therefore, the secondary flux linkage is lower than the primary one so that the mutual inductance $L_{12} = L_{21}$ exceeds the secondary self inductance L_{22} although the turns ratio is equal one. In general not all the flux tubes need to fulfill such condition in order to cause the exceeding. A portion of the flux tubes generated by the secondary winding and satisfying the relation $a_2 < a_1$ can be sufficient to achieve $\Psi_2 < \Psi_1$ which leads to $L_{22} < L_{12}$ and consequently to $I_2 > I_1$.

5.1.2. Secondary conductors with skin effect

In order to investigate the influence of the skin effect on the current ratio we regard a solid secondary winding which is short-circuited while the primary winding is fed by harmonic current $\underline{I}_1$. In order to determine the secondary current $\underline{I}_2$ it is necessary to solve the field problem inside the cross section of forward conductor 2 (see Fig. 8). It is therefore beneficial to represent the harmonic fields by phasors $\underline{H}_y$ and $\underline{E}_z$ according to:

$$H_y(x,t) = \text{Re}\left\{\sqrt{2}\,\underline{H}_y(x)e^{j\omega t}\right\},\ \ E_z(x,t) = \text{Re}\left\{\sqrt{2}\,\underline{E}_z(x)e^{j\omega t}\right\}. \tag{38}$$

Ampere's law and Faraday's law [7] combined with material-specific field relations $\vec{J} = \gamma\vec{E}$ and $\vec{B} = \mu\vec{H}$ yield following equations for $\underline{H}_y$ and $\underline{E}_z$:

$$\begin{aligned} &\text{I}: \quad \nabla\times\vec{H} = \vec{J} \quad \Rightarrow \quad \frac{\partial\underline{H}_y}{\partial x} = \gamma\underline{E}_z, \\ &\text{II}: \quad \nabla\times\vec{E} = -\frac{\partial\vec{B}}{\partial t} \Rightarrow -\frac{\partial\underline{E}_z}{\partial x} = -j\omega\mu\underline{H}_y. \end{aligned} \tag{39}$$

Eliminating $\underline{E}_z$ we receive the governing equation for $\underline{H}_y$

$$\frac{\partial^2\underline{H}_y}{\partial x^2} = \underline{\beta}^2\underline{H}_y\,, \qquad \underline{\beta} = \frac{1+j}{\delta}, \qquad \delta = \sqrt{\frac{2}{\omega\mu\gamma}}\,, \tag{40}$$

the solution of which is [8]

$$\underline{H}_y(x) = \underline{C}_1\sinh(\underline{\beta}x) + \underline{C}_2\cosh(\underline{\beta}x). \tag{41}$$

Substitution of (41) in (39, I) yields the solution for $\underline{E}_z$

$$\underline{E}_z(x) = \frac{\underline{\beta}}{\underline{\gamma}}\underline{C}_1 \cosh\left(\underline{\beta} x\right) + \frac{\underline{\beta}}{\underline{\gamma}}\underline{C}_2 \sinh\left(\underline{\beta} x\right). \tag{42}$$

Now we determine the coefficients $\underline{C}_1$ and $\underline{C}_2$ from the boundary conditions. Considering that the magnetic field vanishes inside the back iron the result is in accordance with Ampere's law:

$$\oint \underline{\vec{H}} \cdot d\vec{l} = \int_{y=0}^{h} \underline{H}_y(x)dy \overset{x=b}{=} \underline{I}_1 \qquad \Rightarrow \qquad \underline{H}_y(b)h = \underline{I}_1. \tag{43}$$

Furthermore, the secondary winding is short-circuited, so the electric field inside is purely induced. Then Faraday's law yields considering symmetry:

$$\begin{gathered} 2 \cdot \int_{z=0}^{l_z} \underline{E}_z(x)dz = 2 \cdot l_z \underline{E}_z(x) = 2 \cdot j\omega\mu\, l_z \int_{\tilde{x}=0}^{x} \underline{H}_y(\tilde{x})d\tilde{x} \overset{x\to 0}{=} 0 \\ \Rightarrow \underline{E}_z(0) = 0. \end{gathered} \tag{44}$$

The conditions (43), (44) lead to the coefficients $\underline{C}_1$ and $\underline{C}_2$:

$$\begin{array}{l} \underline{H}_y(b) = \dfrac{\underline{I}_1}{h} \\ \underline{E}_z(0) = 0 \end{array} \Rightarrow \begin{array}{ll} \underline{C}_1 \sinh\left(\underline{\beta} b\right) + \underline{C}_2 \cosh\left(\underline{\beta} b\right) = \dfrac{\underline{I}_1}{h} \\ \dfrac{\underline{\beta}}{\underline{\gamma}}\underline{C}_1 = 0 \end{array} \Rightarrow \begin{array}{l} \underline{C}_1 = 0 \\ \underline{C}_2 = \dfrac{\underline{I}_1}{h\cosh\left(\underline{\beta} b\right)} \end{array}. \tag{45}$$

The secondary current $\underline{I}_2$ results from Ampere's law analogously to (30):

$$\underline{I}_1 + \underline{I}_2 = h \cdot \underline{H}_y(0) = h \cdot \underline{C}_2 \quad \Rightarrow \quad \underline{I}_2 = h \cdot \frac{\underline{I}_1}{h\cosh(\underline{\beta} b)} - \underline{I}_1 . \tag{46}$$

We finally receive following expression for the current ratio:

$$\frac{I_2}{I_1} = \left| \frac{1}{\cosh\left(\underline{\beta} b\right)} - 1 \right| = \left| \frac{1}{\cosh\left((1+j) \cdot b/\delta \right)} - 1 \right|. \tag{47}$$

The resulting curve is depicted in Figure 11. In case the secondary winding is solid and consequently the skin effect occurs, the current ratio grows in the low frequency range and achieves a pronounced local maximum of value > 1. However, with growing frequency the current density and consequently the effective current-carrying-cross-section of the secondary winding increasingly concentrates near the primary winding. Thereby the portion of the interior flux, responsible for the phenomenon, decreases for the effective (!) cross-section and the current ratio tends to the value of one at high frequency.

The same physical explanation is valid for the arrangement in Figure 1. In particular the frequency response of the current ratio I_2 / I_1 which was determined there is very similar to the curve from Figure 11 (with skin effect).

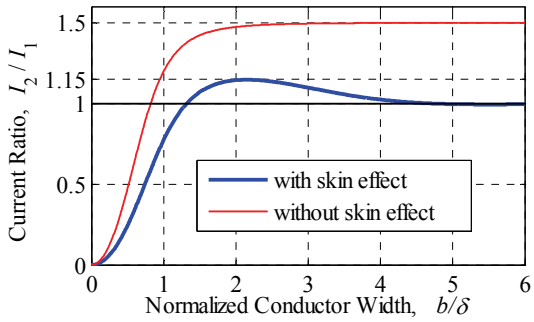

Fig. 11. Current ratio of the arrangement according to Fig. 8 as a function of parameter b/δ which grows with increasing frequency ($b/\delta \sim f^{1/2}$)

6. An example with higher mmf-ratio

In the previous sections the phenomenon $I_2 / I_1 > 1$ turned out to be caused by the circumstance, that a part of flux tubes is linked with the secondary winding partially (interior flux) and with the primary winding fully (exterior flux) simultaneously. The arrangement according to Figure 11 reaches the value of $I_2 / I_1 = 1.5$ (without skin effect). Now the question is whether this value can be raised markedly by changing geometry which is crucial for the ratio I_2 / I_1 since it has an impact on the flux linkages. And the answer is yes, which is proved by the rotationally symmetric arrangement shown in Figure 12.

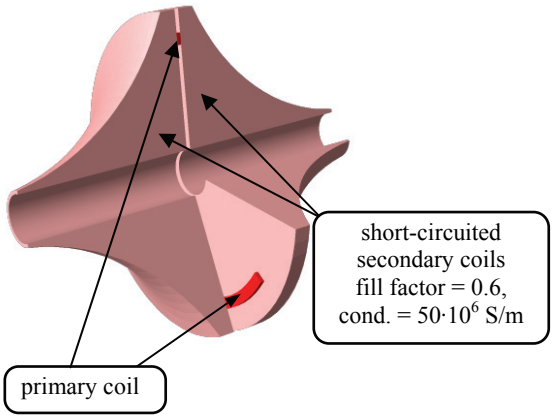

Fig. 12. Rotationally symmetric arrangement with high peak ratio I_2 / I_1

The secondary winding consists of two equal, short-circuited coils (no skin effect!). Due to the very small inside radius (r_i / r_a = 2 mm/14 mm) as well as absence of skin effect nearly complete flux of the secondary coils is interior. Additionally the linkage of this flux with the secondary cross-section is reduced by its geometric profile. The primary coil has a small

cross-section which is arranged in such a way that it is linked with as many flux tubes as possible (see Fig. 13) in order to increase the mutual inductance.

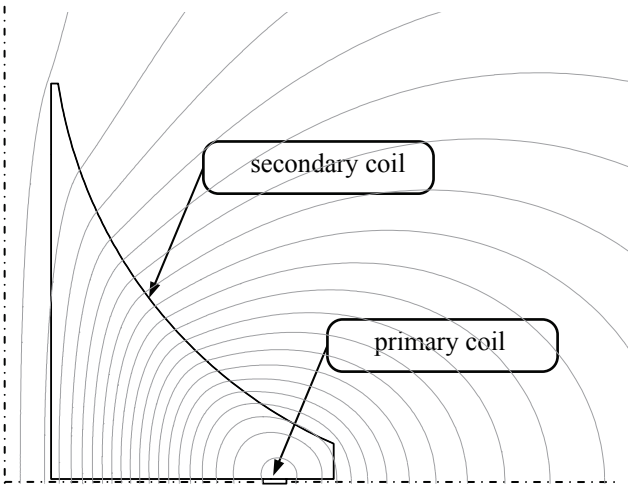

Fig. 13. Flux tubes produced by the secondary coils. The flux linkage with the primary coil is full but with the secondary-coil-cross-section only partial

The frequency response of the ratio I_2 / I_1 is determined by (28). Consequently for small frequencies the ratio tends to zero due to the resistance $R_2 > 0$, which results from the finite conductivity of the coil wire (see Fig. 12). With growing frequency the ratio I_2 / I_1 converges to the value L_{21} / L_{22}. The curve resulting for the rotationally symmetrical arrangement is depicted in Figure 14.

As we can see, the maximum of the ratio I_2 / I_1 is in fact markedly greater than in the examples from section 6 and amounts to a value of 2.25 when the frequency is higher than approximately 5000 Hz. So the mmf of a short-circuited coil can reach more than double value of the exciting mmf.

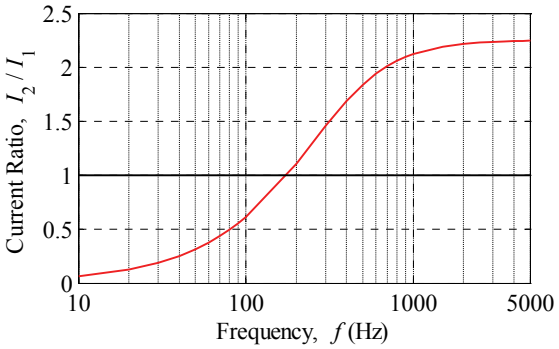

Fig. 14. Current ratio of the rotationally symmetric arrangement (see Fig. 12)

7. Conclusion

In general the eddy current or the mmf of a short-circuited loop can markedly exceed the mmf exciting it. In case of eddy current the mmf-ratio-frequency-response reaches local maximum > 1 at a certain frequency and falls to a value < 1 for higher frequencies. In case of a stranded secondary winding the mmf ratio tends monotonously to a value > 1 with growing frequency. Mmf of a solid conductor exceeds the exciting mmf weaker than that of a stranded one. This results from the skin effect which reduces the percentage of interior flux that causes the exceeding.

References

[1] Kriezis E.E., Tsiboukis T.D., Panas S.M., Tegopoulos J.A., *Eddy Currents: Theory and Applications*, Proceedings of the IEEE 80: 1559-1589 (1992).
[2] Schunk H., *Stromverdrängung*. Dr. Alfred Hüthig Verlag (1974).
[3] Smythe W.R., *International Series in Pure and Applied Physics, Static and Dynamic Electricity, Third Edition*, McGraw-Hill, pp. 368-414 (1968).
[4] Stoll R.L., *The Analysis of Eddy Currents*, Clarendon Press, Oxford (1974).
[5] Tegopoulos J.A., Kriezis E.E., *Studies in Electrical and Electronic Engineering*. Bd. 16: *Eddy Currents in Linear Conducting Media*, Elsevier (1985).
[6] Bewley L.V., *Two-dimensional fields in electrical engineering*, Dover Publications, Inc., New York, pp. 73-81 (1963).
[7] Simonyi K., *Theoretische Elektrotechnik*, 5. Auflage, VEB Deutscher Verlag der Wissenschaften, Berlin (1973).
[8] Bronstein I.N., Semendjajew K.A., *Taschenbuch der Mathematik, 2. Auflage*, Verlag Harri Deutsch (1995).